

CONFIRMATION OF A STEEP LUMINOSITY FUNCTION FOR Ly α EMITTERS AT $z = 5.7$: A MAJOR COMPONENT OF REIONIZATION*

ALAN DRESSLER

Carnegie Observatories, 813 Santa Barbara St., Pasadena, California 91101-1292

ALAINA HENRY

Astrophysics Science Division, Goddard Space Flight Center, Code 665, Greenbelt, MD 20771

CRYSTAL L. MARTIN

University of California, Santa Barbara, Department of Physics, Santa Barbara, CA 93106

MARCIN SAWICKI

St. Mary's University, Department of Astronomy and Physics, 923 Robie Street, Halifax, N.S., B3H 3C3, Canada

PATRICK MCCARTHY

Carnegie Observatories, 813 Santa Barbara Street, Pasadena, California 91101-1292

EDWARD VILLANEUVA

Carnegie Observatories, 813 Santa Barbara Street, Pasadena, California 91101-1292

Submitted: 2014 September 15

ABSTRACT

We report the first direct and robust measurement of the faint-end slope of the Ly- α emitter (LAE) luminosity function at $z = 5.7$. Candidate LAEs from a low-spectral-resolution blind search with IMACS on Magellan-Baade were targeted at higher resolution to distinguish high redshift LAEs from foreground galaxies. All but 2 of our 42 single-emission-line systems are fainter than $F = 2.0 \times 10^{-17}$ ergs s $^{-1}$ cm $^{-2}$, making these the faintest emission-lines observed for a $z = 5.7$ sample with known *completeness*, an essential property for determining the faint end slope of the LAE luminosity function. We find 13 LAEs as compared to 29 foreground galaxies, in very good agreement with the modeled foreground counts predicted in Dressler et al. (2011a) that had been used to estimate a faint-end slope of $\alpha = -2.0$ for the LAE luminosity function. A 32% LAE fraction, LAE/(LAE+foreground) within the flux interval $F = 2-20 \times 10^{-18}$ ergs s $^{-1}$ cm $^{-2}$ constrains the faint end slope of the luminosity function to $-1.95 > \alpha > -2.35$ (1σ). We show how this steep LF should provide, to the limit of our observations, more than 20% of the flux necessary to maintain ionization at $z = 5.7$, with a factor-of-ten extrapolation in flux reaching more than 55%. We suggest that this bodes well for a comparable contribution by similar, low-mass star forming galaxies at higher-redshift — within the reionization epoch at $z \gtrsim 7$, only 250 Myr earlier — and that such systems provide a substantial, if not dominant, contribution to the late-stage reionization of the IGM.

Subject headings: galaxies: high-redshift – galaxies: evolution – galaxies: formation

1. INTRODUCTION

Our understanding of galaxy evolution during the epoch of reionization has improved with the deep near-IR imaging from WFC3 on the Hubble Space Telescope. Numerous *Lyman-break* galaxies (hereafter, LBGs) have been found at redshifts $z = 6-9$, with a *luminosity function* (hereafter, LF) that spans a factor of ~ 100 in brightness (e.g., McLure et al. 2013; Ellis et al. 2013; Bouwens et al. 2014; Oesch et al. 2014). Although the photometric redshifts of these young galaxies are reasonably secure, spectroscopic confirmation of

Ly α emission has proven elusive in most cases (Fontana et al. 2010; Pentericci et al. 2011; Schenker et al. 2012; Caruana et al. 2012, 2014; Bunker et al. 2013). There is mounting evidence that this is due to a significant fraction of remaining HI that substantially attenuated any Ly α emission escaping these young objects (Stark et al. 2010; Ono et al. 2012; Treu et al. 2013; Tilvi et al. 2013; Momose et al. 2014; cf. Dijkstra et al. 2014).

Young stellar populations in early galaxies were the likely sources of high-energy ($E > 13.6$ eV) photons responsible for reionization of the intergalactic medium (IGM). However, it is well known that the brighter galaxies provided a small fraction of the required flux, so that much larger numbers of fainter, unobserved galaxies would be needed to balance or exceed the ionizing budget (Bunker et al. 2010). In fact, recent surveys that reach deeper do suggest that the LF of Lyman-break galaxies is steep, with faint-end slope $\alpha \sim -2.0$

*This paper includes data gathered with the 6.5 meter Magellan Telescopes located at Las Campanas Observatory, Chile.

Electronic address: dressler@obs.carnegiescience.edu

Electronic address: alaina.henry@nasa.gov

Electronic address: cmartin@physics.ucsb.edu

Electronic address: sawicki@ap.smu.ca

Electronic address: pmc2@obs.carnegiescience.edu

Electronic address: edwardv@obs.carnegiescience.edu

(Bradley et al. 2012; Alavi et al. 2014; Schmidt et al. 2014; Bouwens et al. 2014). The observed galaxies alone account for approximately 10% of the required Lyman-continuum flux: if a slope of $\alpha \sim -2.0$ continues to a luminosity ~ 10 -100 times lower, then these galaxies should account for a substantial fraction of the flux required for full reionization (Robertson and Ellis 2012; Robertson et al. 2013; Schmidt et al. 2014).

On the other hand, it is not clear that Lyman-break galaxies can supply sufficient Lyman-continuum photons into the IGM. Even at lower redshifts, $z = 5 - 6$, where neutral hydrogen is gone from the IGM, Ly α emission is only sometimes detected in Lyman-break galaxies (e.g., Shapley et al. 2003; Kornei et al. 2010; Stark et al. 2010; cf. Curtis-Lake et al. 2014), as it of course is for the class of galaxies *defined* by strong emission — the *Ly α -emitters* (LAE). As described by Schaefer (2014), LAEs and LBGs at high redshift are closely related star forming systems whose differences in observable properties could be due entirely to differences in dust content. The lower (on-average) stellar mass of LAEs compared to LBGs may be connected to their systematically lower dust contents. It is possible, then, that the mature stellar populations in Lyman-break galaxies, evident in their strong stellar UV-continua, entrain enough dust to prevent many Ly α photons, and most Lyman-continuum photons, from leaving the galaxy. For example, from observations of LBGs and LAEs at $z \sim 3$, Nestor et al. 2013 find Lyman-continuum escape fractions 2-4 times higher than for LAEs. For this reason, the needed Lyman-continuum photons may preferentially come from LAEs, where stellar continuum radiation is weak, and the dominance of emission is the signature of a younger starburst — perhaps the first major episode of star formation in the system.

The largest collections of LAEs at $z > 5$ come from narrow-band imaging surveys with the Subaru telescope (e.g., Shimasaku et al. 2006; Ouchi et al. 2008; Hu et al. 2010; Kashikawa et al. 2011). With the wide field-of-view of the SuprimeCam, narrow-band searches are an efficient way to find high redshift LAEs with luminosities $L \gtrsim L^*$, $\approx 10^{43}$ ergs s $^{-1}$. Thus, these studies have a good purchase on two of the Schechter function parameters, Φ^* and L^* , within their significant covariance. However, as explained in Dressler et al. (2011a), MNS2) and reiterated in §3.2 of this paper, detections of LAEs below L^* become rapidly incomplete for narrow-band observations of ~ 150 Å FWHM. Although some fainter objects are detected, incomplete sampling makes such data at $z = 5.7$ unsuitable for measuring the faint-end slope α .

Our *Multislit Narrowband Survey*, hereafter MNS, was specifically designed to produce complete samples of LAEs up to ten-times fainter than the narrow-band imaging surveys. Basically, this is accomplished by searching the same low-OH-background part of the spectrum as for imaging surveys for $z = 5.7$ LAEs (8110–8270 Å), but by adding a grism to disperse the light so that each emission-line-detection competes against a ten-times-lower sky background. The origin of the technique, and our application of it using the 27 arcmin-diameter field of the IMACS f/2 channel, is detailed in Martin et al. (2008, MNS1) and in MNS2.

MNS2 describes the analysis of an excellent observing run in 2008 that produced ~ 20 hours of integration for each of two fields, netting a sample of 210 single-emission-line, no-detected-blue-continuum sources that were candidate LAEs at $z = 5.7$. These spectra reached a 50% completeness at a line

flux of $F = 3.5 \times 10^{-18}$ ergs s $^{-1}$ cm $^{-2}$, sufficiently faint for the first credible measurement of the faint-end-slope of the LAE luminosity function (hereafter, LF). However, because of the relatively low spectral resolution of ≈ 10 Å FWHM and the ~ 150 Å coverage of the search spectra, LAEs could not be reliably separated from foreground galaxies producing [O II], [O III], H β , or H α emission, which together were expected to outnumber the LAEs by about 2-to-1. In MNS2 we used published results of counts of these foreground sources — extrapolated to the fainter limits of the MNS survey — to statistically correct for the foreground contamination and construct the residual LAE LF. This process depended most sensitively on the faint-end slope of each of the foreground populations, whose value and range we needed to estimate. Our best estimates of these quantities led to a faint-end slope of the LAE LF of $\alpha = -2.0$, but values as low as -1.5 or as high as -2.5 could not be ruled out.

Confirmation of a steep slope for LAEs at $z \sim 6$ has important implications for questions of galaxy formation, the production of heavy elements in the universe, and reionization, so we have been strongly motivated to confirm the result of a steep slope of the LAE LF forecast by our statistical correction for foreground contamination. Accomplishing this requires higher dispersion spectra for a statistically significant sample of the faintest LAE candidates. Our first efforts to do this have been described in Henry et al. (2012, MNS3), where LAEs were positively identified in the COSMOS field using spectra from Keck-DEIMOS with a resolution of $\lambda \approx 2$ Å; these results are briefly reviewed in §4.1. In this paper we present similar spectra for a significantly larger sample of faint LAEs in our 15h field (LCRIS), leading to a determination $\alpha = -2.15 \pm 0.20$, in good agreement with the results of MNS2.

The paper is organized as follows: §2 describes the new data taken with IMACS on Magellan; §3 describes how these objects were matched to those found in the low-resolution search, and the criteria for separating LAEs from foreground galaxies; §4 explains how we used these data to constrain the faint-end slope of the LAE LF; §5 explores the implication of this now-confirmed steep slope of the LAE LF for reionization; and §6 gives our conclusions.

2. THE DATA: HIGHER DISPERSION SPECTRA OF CANDIDATE LAES

The experimental technique of the 2008 MNS search was to use 100 parallel long slits crossing the full field of view of the IMACS f/2 camera, a circle of 27 arcmin diameter. The spacing was chosen to allocate about ~ 70 pixels in the dispersion direction per slit, which covered a “low-OH-emission” spectral band of $\lambda = 8115 - 8250$ Å at 2.0 Å pix $^{-1}$. The 2008 MNS search used this setup, described in MNS2, to cover ~ 55 sq arcmin ($\sim 10\%$ of the full f/2 imaging field) in both the COSMOS field and the Las Campanas Redshift Survey field (Marzke et al. 1999). Slits 1.5 arcsec wide produced a spectral resolution of 14 Å for objects that fill the slits, but for the typical size and profile of the discovered single-line sources, and the good seeing conditions of the search (< 0.6 arcsec FWHM) a 10 Å FWHM resolution was typical. Still, at this resolution, spectra of LAEs are usually indistinguishable from single-emission-line foreground galaxies, since a resolution of less than $\lesssim 5$ Å is required to resolve the characteristic asymmetry of most Ly α emission lines, or to split the doublet of [O II] foreground sources at $z \approx 1.20$. Because these

data could not be used to unambiguously identify the LAEs at $z \approx 5.7$, the result from MNS2 of a steep slope of $\alpha \approx -2.0$ for the LAE LF depended on a statistical correction for the foreground contamination. Since this further depended on an extrapolation of the LFs for foreground sources to fainter limits than observed, the putative steep slope of MNS2 required further spectroscopy, to identify LAEs on an individual basis.

Such follow up spectral observations at 2-3 Å FWHM resolution were planned with both IMACS and Keck-DEIMOS starting in 2010. Observations planned in 2010, 2011, and 2012 for IMACS on Magellan-Baade were thwarted by poor weather, but observations in 2010 and 2011 with DEIMOS of LAE candidates in the COSMOS field were moderately successful in terms of observing conditions. The DEIMOS observations confirmed 6 LAEs from the faint sample; the basic results of MNS3 are reviewed in §4.1.

In April 2013 and March 2014, two mostly-clear 5-night runs at Las Campanas Observatory, with average, on-target seeing of 0.68 arcsec and 0.71 arcsec (approximately the median seeing at Magellan), were successfully completed using IMACS in f/4 mode (Dressler et al. 2011b) with a 600-l/mm +13° blaze grating, delivering a scale of 0.378 Å pix⁻¹ and a spectral resolution (1.0 arcsec-wide slit) of ~ 3 Å. The detector readout was rebinned by a factor-of-two in the spatial direction to increase signal over read noise, resulting in a scale of 0.22 arcsec pix⁻¹. A single slit mask was designed and fabricated for each year; each mask targeted LAE candidates in the 15h field of the *Las Campanas Redshift Survey* (Marzke et al. 1999). The position angle of slits was rotated by 90° from that of the long slits in the 2008 search mask, in order to place *along* the slit the coordinate that includes a degeneracy between sky position and line wavelength. The multi-slit masks of the IMACS f/4 cover a field of 15 arcmin x 15 arcmin. For the 2013 and 2014 runs, total integration times were 27.4 and 17.5 hours, respectively. The spectral range extended out to 9000 Å for all spectra, and for most extended down to ~ 6000 Å, important for confirming those cases where H α was the line detected in the search window.

The new IMACS f/4 spectra were reduced using the *COSMOS* software package — <http://code.obs.carnegiescience.edu/cosmos/Cookbook.html>, augmented by programs written in Python by Kelson that facilitated the reduction of emission-line only sources, a departure from the common data reduction with *COSMOS* that makes use of object continua for fine-tuning object detection. Wavelength calibration and registration were performed using He+Ne+Ar lamp spectra taken in proximity to each set of science frames, while the modeling and subtraction of sky was done using the Kelson (2003) procedure. The reductions produced 2D frames of sky subtracted spectra that were shifted and added using *IRAF* ‘imcombine’ to produce a single frame for each year’s observations. These were examined with *Viewspectra*, a *COSMOS* routine for interactive examination of 2D spectra and for extracting 1D spectra.

Redshifts were measured for 45 of the 52 LAE candidates (“single-emission-line, no-blue-continuum sources” — see MNS2), an 87% success rate of recovering the targets from the 2008 search catalog. The other 13% failed to show an emission-line at or near the predicted spatial or wavelength position; in fact, none of these showed a convincing line over the full wavelength band. Twelve of the 52 candidates were repeated in the 2014 spectroscopy. Nine of the repeats

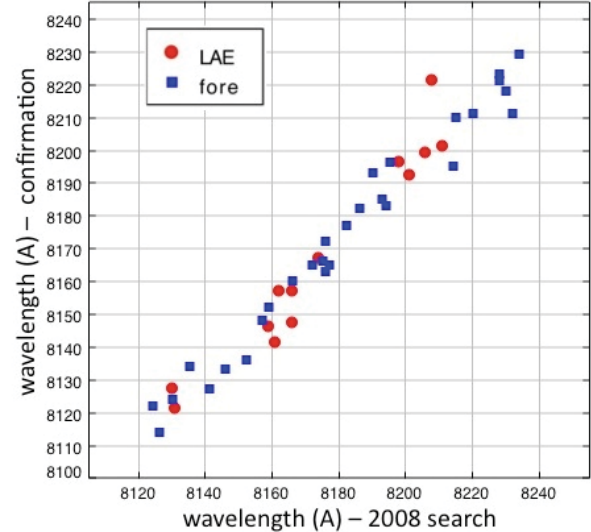


FIG. 1.— Wavelengths of single-emission-line sources from the 2008 search for faint LAEs compared to confirmation observations with higher spectral dispersion in 2013 and 2014. The dispersion and offset is dominated by uncertainties in the 2008 search data, for which wavelength calibration is difficult. The apparent clumping of the LAEs into three systems with a typical separation of ~ 200 km s⁻¹ is likely to be real and indicative of a significant cosmic variance.

were recovered spectra in good agreement with the 2013 data, while for three no object was found, as in 2013.

3. RESULTS

The final sample consists of 45 spectra: 13 sources are identified as LAEs and 32 as foreground galaxies (identified through criteria described below). For 3 of foreground galaxies the recovered emission line was an order-of-magnitude brighter than that of the 2008 candidate.¹ These were judged to be cases where the LAE candidate was actually an HII region of a foreground galaxy, and the galaxy to which it belonged revealed when the slit orientation was changed by 90° to remove the wavelength-position ambiguity (see §2). Also, two of the foreground galaxies are excluded from the following analysis because, though they are confirmations of the 2008 candidate data, they have fluxes of $F = 27$ & 84×10^{-17} ergs s⁻¹ cm⁻²: this is a factor-of-ten brighter than the flux interval we are interested in. The probability of finding a LAE this bright is less than 1% for the area covered by our survey. This leaves a sample of 13 LAEs and 27 foreground galaxies covering the range in flux $F = 2-20 \times 10^{-18}$ ergs s⁻¹ cm⁻², the relevant range for the determination of the faint-end slope of the luminosity function (fainter than L^{*}), as can be seen in Figures 10 and 11 of MNS2.

Concerning the measured fluxes of these sources, we note that photometry is problematical with spectroscopic data, due to the uncertainty of object position with respect to slit and the fact that some objects are bigger than the slit width (slit losses). For the faint objects of our study, sky subtraction and flat-fielding errors add to the difficulty. Furthermore, those at the flux limit of our sample, $F \sim 3 \times 10^{-18}$ ergs s⁻¹ cm⁻², are only S/N $\approx 3-4$ detections (see MNS2, Figure 3). The combined effect, evident in comparing our 2008, 2013, and 2014 data sets, is that photometry accurate to $\lesssim 10\%$ is not possible — typical errors are typically two or three times larger.

¹ One of these was at the wrong spatial position and another had a strong continuum as well.

In MNS3 we implemented a maximum-likelihood methodology capable of deriving the luminosity function in the presence of such photometric scatter and the uncertain positions of objects within the slits of the blind search. In this paper we take an alternative approach based on the LAE fraction which, as we show in §4, is also robust to these effects.

We retained the fluxes measured from the 2008 search spectra for the following analysis, however, among the 27 foreground sources of the final sample (but for none of the LAE sample) 4 objects were significantly brighter in the 2013, 2014 spectroscopy than in the discovery spectra, 2 by $\sim 30\%$ and 2 by a full factor-of-two. We judged these to be cases of slit-losses in the discovery spectra — a reasonable fraction — and revised them to the higher value.

3.1. Criteria for discriminating $z = 5.7$ LAEs from foreground galaxies

We have a high degree of confidence in the sample of LAEs we report here. The criteria that underlie this confidence is a series of qualifications. First, to be considered a "recovered candidate" from the the 2008 search, an emission line in the 2013 and/or 2014 spectra must agree with the wavelength found in the search data. Figure 1 shows this comparison for both the LAEs and foreground sources in the new data. Compared to the $\sim 120\text{\AA}$ range of the bandpass, the $\sim 5\text{\AA}$ scatter in the relation is small, ergo, there is no question that the recovered objects are the ones found in the 2008 search.² The recovered spectra were also required to lie within ± 2 arcsec of the spatial position on the slit predicted from the 2008 search data.

Second, all the foreground objects are easily identified through their spectral signatures. Figure 2 shows extracted spectra from the 2D data. [O II] emission at $z \approx 1.20$ accounts for $\sim 60\%$ foreground contamination. As shown in the middle panel, the [O II] doublet is well-resolved and the lines easily distinguished, even for the faintest objects. Emission-line galaxies at $z \approx 0.64$ are also a major component of the foreground: the $\lambda 5007$ line of [O III] is shown for 6 out of the 8 cases (right-hand column of Figure 2) and in all these cases $\lambda 4959$ is also detected, and usually $\text{H}\beta$ as well. $\text{H}\alpha$ at $z = 0.25$ and $\text{H}\beta$ at $z \approx 0.68$ accounts for only 10% of the foreground, and only one of these show accompanying [N II] emission, but in all but one case $\text{H}\alpha$ is ruled in or out by the detection of [O III] at an observer-frame wavelength of $\sim 6250\text{\AA}$. A rare [Ne III] line, confirmed by the presence of [O II], was also found, but together [O II], [O III]/ $\text{H}\beta$, and $\text{H}\alpha$ should account for 99% of the foreground, since these are much stronger than any other lines from [O II] to $\text{H}\alpha$. $\text{H}\gamma$ or $\text{H}\delta$ emission could have been found, but [O II] would always accompany them.

The remaining 13 emission lines are identified as $\text{Ly}\alpha$, shown in the left column of Figure 2. The characteristic asymmetry of $\text{Ly}\alpha$ is seen in 8 of the 13 objects, and 3 others, although not clearly asymmetric at this signal-to-noise, are

² The dispersion in wavelength, as well as the $\sim 10\text{\AA}$ shift between the search data and the follow-up data is dominated by the former. Repeat measurements in 2014 of 12 objects observed in 2013 show a typical error of less than 1\AA , from well-calibrated arc lines spanning of several thousand angstroms. There are no comparison arc lines in the narrow band of the 2008 search data, which covers only $\sim 150\text{\AA}$. We used the narrow-band interval itself to define the wavelength scale, but the bandpass shifts with angle from the optical axis, and the "venetian blind" mask made used in the LCRIS (15h) search added additional uncertainty because of departure from sphericity of the highly perforated mask, another source of error in the wavelength.

clearly too broad to be foreground lines: [O III]/ $\text{H}\beta$, $\text{H}\alpha$ — are all ruled out, as described above, and the small velocity broadening expected for these foreground dwarf galaxies ($M \sim -17$), $\sigma \lesssim 50 \text{ km s}^{-1}$, rules out the possibility of broadened [O II]. Three additional $\text{Ly}\alpha$ lines are narrower: they resemble those of fainter LAEs from the Subaru-SuprimeCam studies (Kashikawa et al. 2011) and two examples from our own Keck-Deimos spectra (MNS3). For the three found here, labeled 1.9, 2.6, and 3.5 in Figure 2, [O II], [O III]/ $\text{H}\beta$, and $\text{H}\alpha$ (by lack of [O III] emission, see above) are all ruled out.

In summary, we consider these 13 $\text{Ly}\alpha$ identifications to be secure, and the foreground identifications as well.

Basic data for these 13 LAEs, including positions, are given in Table 1.

3.2. These are the faintest LAEs yet detected at $z \sim 6$

All 13 LAEs are fainter by a factor of 2 to 5 than the completeness limits of two Subaru Suprime-Cam narrow-band surveys, COSMOS $F \approx 2 \times 10^{-17} \text{ ergs s}^{-1} \text{ cm}^{-2}$, and the Subaru Deep Field, $F \approx 1.6 \times 10^{-17} \text{ ergs s}^{-1} \text{ cm}^{-2}$ (see Figure 1 of Takahashi et al. 2007). Although Kashikawa et al. (2011) include LAEs 2-3 times fainter than these limits, the detections have large errors, $S/N < 3$, with the result that they are drawn from a very incomplete sample. For this reason, the faint-end slope of the LAE LF is unconstrained by the Subaru narrow-band data, as is apparent from the renderings of the LF in Kashikawa et al.'s Figures 7 & 9. Our MNS study has the only sample of LAEs that constrains the faint end slope of the LAE LF at $z = 5.7$.

4. MEASURING THE SLOPE OF THE LAE LUMINOSITY FUNCTION

The slope of the LAE LF is the critical determinant of the contribution of low-luminosity LAEs to reionizing flux in the early universe. Uncertainties in the other Schechter function parameters — a lower characteristic luminosity L^* or even a lower space density Φ^* — are quickly overcome if the slope is steep, $\alpha < -1.5$, needing only a factor-of-two more "depth" to reach the photon flux capable of reionizing the universe.

In MNS2 we presented a sample of 210 galaxy spectra that showed only a single emission line in a 140\AA -wide search band centered at $\lambda \approx 8180\text{\AA}$. The source counts of these candidate LAEs rose rapidly with decreasing flux, but we recognized that most of these sources had to be foreground galaxies. Lacking the high-resolution spectra we now have (or any reliably way separate LAEs from foreground), we used published data from Taniguchi et al. (2007) of foreground [O II], [O III], and $\text{H}\alpha$ emitters to remove the foreground statistically, leaving a possible LAE LF. In particular, subtracting our best Schechter-function fits to the foreground counts (shown in Figure 8 of MNS2) produced an LAE LF with a faint end slope $\alpha \approx -2.0$ that matched up well with an LAE LF with the same slope from Shimasaku et al. 2006 (see MNS2, Figure 10) — one of three acceptable fits to the LAE LF they made using their sample of $L \gtrsim L^*$ LAEs.

Unfortunately, the LAE LF we derived with this method was not unique: our Schechter fits to the LFs of the 3 foreground populations could not be tightly constrained because they required an extrapolation to the faint flux levels of our study: the Taniguchi et al. data come from narrow-band imaging observations that, like the LAEs, become rapidly incomplete for $\log F < -17.0$. For this reason, we needed to consider perturbations on the "best-fitting" foreground LFs to assess the robustness of our result of an LAE LF with slope $\alpha = -2.0$.

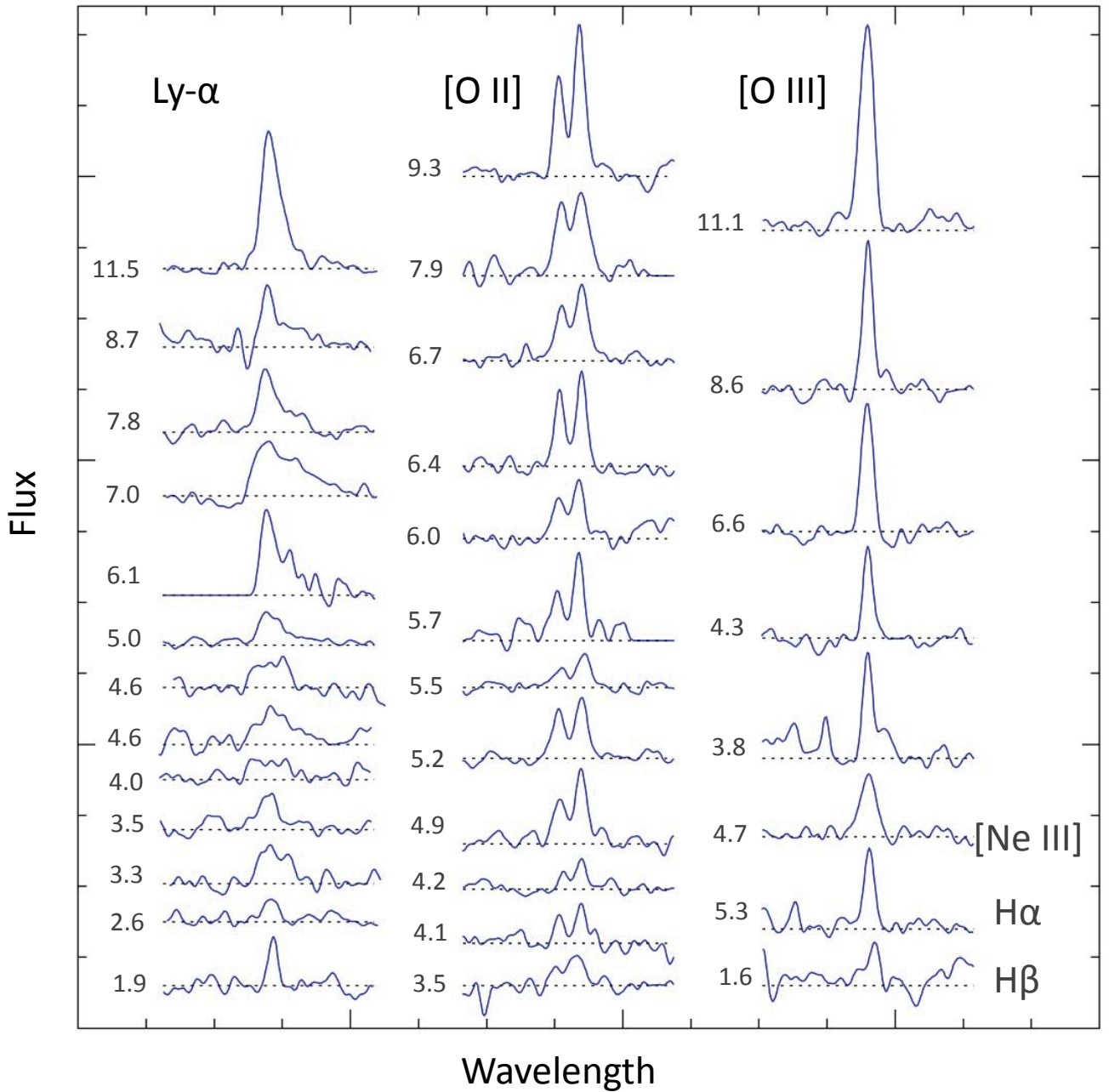


FIG. 2.— Spectra of LAE candidates from 2013 and 2014 observations with IMACS on Magellan-Baade. The number to the left of each spectrum is its flux in units of 10^{-18} ergs s^{-1} cm^{-2} . The left column shows the 13 detected LAEs at $z \approx 5.7$. The middle column shows 12 of the 16 detected [O II] emitters at $z \approx 1.20$, which account for $\sim 60\%$ of the foreground sample. The third column shows 8 of the remaining 11 foreground spectra, 6 of the 8 detected [O III] emitters ($z \approx 0.64$, $\sim 30\%$ of the foreground) and the three remaining foreground sources, H α , H β , and [Ne III].

In that exercise, we learned that we could not rule out a much shallower slope for the LAE LF, even to $\alpha = -1.0$, or even a slope as steep as $\alpha = -2.5$. Here we use the term “realization” to refer to each of the possible LAE LFs we generate by modifying the foreground LFs within their uncertainties. In the process of making such realizations in MNS2, we also found — not surprisingly — that the fraction of LAEs, LAE/(LAE+foreground) was a sensitive function of the LAE LF slope. The power of the new data presented in this paper is

that even a small sample of 40 LAE+foreground sources can greatly reduce the range of acceptable realizations. This is the approach that we now describe.

In MNS2 we adopted the Shimasaku et al. Schechter LF fits to their LAE data³ with faint end slopes of -1.0, -1.5, and -2.0, as models for the different “realizations” of the LAE LF we had made by subtracting slightly different levels of fore-

³ Parameters for these LFs are closely matched by those in Hu et al. (2010).

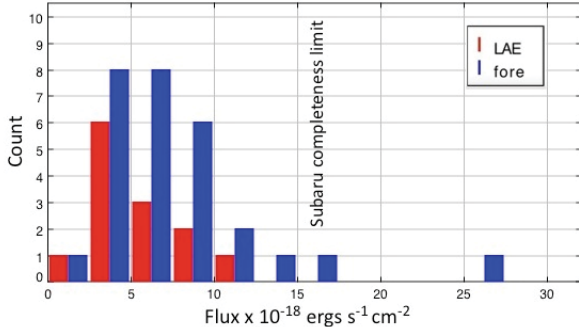


FIG. 3.— Flux distribution for LAE and foreground sources, showing the increasing fraction of LAE compared to the foreground population with decreasing flux.

ground contamination. This means that each realization was made to match a Shimasaku et al. LF of slope α , including its Φ^* ‘normalization.’ The Shimasaku et al. LFs predict 16–18 bright LAEs ($\log F > -17.0$) — depending on the slope — over the volume of our survey (see MNS2 Figure 10). A deficiency of that analysis, however, was the graphical, rather than analytical, comparison of our realizations of the LAE LF with the Shimasaku et al. models (MNS2 Figure 11). We rectify this here by measuring the steepness of the cumulative LAE LF in the Shimasaku et al. models, $R = N_{LAE}(\log F > -17.6)/N_{LAE}(\log F > -17.3)$ — the ratio of the integrated LAE counts over this flux interval, and adjusting the foreground LF fits (within their uncertainties) to achieve the same quantity for each LAE LF realization.⁴ (Each realization also matches the Φ^* normalization discussed above.) Table 2 lists the R values for each model and realization and the values of α , $\log L^*$, and $\log \Phi^*$ for [O II], [O III], and H α foregrounds that were used to achieve the match.⁵

If we now calculate LAE/(LAE+foreground) — the LAE fraction — over the interval $F = 2-20 \times 10^{-18}$ ergs $s^{-1} cm^{-2}$, for each of these three realizations, we find values of 0.099, 0.142, and 0.260, corresponding to an expected number of LAEs of approximately 4, 6, and 10, respectively, for a 40-object sample. These are to be compared with the 13 we actually found. In the next section we describe a simple test of the likelihood of these and other realizations that, in the end, constrain the allowable realizations to a small range of slopes.

4.1. The LAE fraction of different realizations and comparison with observations

In §3 we discussed the substantial uncertainties in the fluxes of our faint sources. Even at this level of accuracy, the data are probably good enough to fit a Schechter function — as we did in MNS3, but in this paper we use a new method that is robust to photometric errors, measuring only the LAE fraction LAE/(LAE+foreground) over a flux inter-

⁴ R is a proxy for the asymptotic slope α , which our data — although well below L^* — do not reach.

⁵ Allowing for cosmic variance in the Φ^* normalizations of the foreground LFs is necessary to reproduce physically meaningful LAE LFs, that is, without negative LAEs or an LF that diverges with increasing depth. Although cosmic variance of order 30% is expected for the combined foreground populations, in this case we made changes in Φ^* of only $\leq 10\%$ from the LFs we adopted from Taniguchi et al. (2007). This was expected, since these LFs were made in one of our fields, COSMOS, and the LCRIS and COSMOS fields have similar distributions of number counts versus flux (compare Figures 1 and 2 in MNS2). The method would work in another field with significantly different levels of the foregrounds, and would produce $z = 5.7$ LAE LFs with the appropriate cosmic variance of $\sim 20\%$ for fields of this size.

val, $F = 2-20 \times 10^{-18}$ ergs $s^{-1} cm^{-2}$, and comparing this with expectations based on luminosity functions of varying slopes. This ratio is well measured — despite the uncertainty in fluxes — because both LAEs and foreground galaxies are well bounded, on the faint end by the flux limit of all detections, and on the bright end by L^* for both LAEs and foreground. Figure 3 shows that for $F > 2 \times 10^{-17}$ ergs $s^{-1} cm^{-2}$ there is only one foreground galaxy out of the total sample of 27, and no LAEs.

Table 3 lists realizations of the MNS2 data we made for the 3 Shimasaku et al. models but also spanning the full range of plausible faint-end slopes, $-1.5 > \alpha > -2.5$, in steps of 0.1. These interpolated Shimasaku et al. models were generated by quadratic fits to $\log \Phi^*$ and $\log L^*$, each as a function of α , based on the three models of slope $\alpha = -1.0$, -1.5 , and -2.0 . Table 3 lists these Schechter function parameters for each model and its R value, which is compared to the R value of the realization of the data that matches this model. With this full range of realizations of the 2008 data, each matching a Shimasaku et al. LAE LF, we use our new data to test the likelihood of each. This was done by calculating the predicted LAE fraction, LAE/(LAE+foreground), over the range $F = 2-20 \times 10^{-18}$ ergs $s^{-1} cm^{-2}$ for each realization, and comparing it to the LAE fraction of our new data, 13/40, or 0.325.

We use a Monte Carlo test to determine how often the observed LAE fraction of 0.325 would be reproduced in each of our realizations of the LAE LF — these results are shown in Table 3. For example, the LAE LF realization with $\alpha_{LAE} = -1.0$ has an LAE fraction of 0.099 — 4 LAEs out of 40 total (single-emission-line-only) detections for this nearly flat slope. The Monte Carlo test uses a random draw from a 40 object sample to determine that the observed number of 13 LAEs would be found only once in 10,000 trials if only 4 are expected. This possible LAE LF is therefore ruled out. The slopes -1.5 and -2.0 , considered in MNS2, have LAE fractions of 0.142 (~ 6 LAEs) and 0.260 (~ 10 LAEs), corresponding to probabilities of 0.19% and 22%, of finding at least 13 LAEs. The ‘best fit’ of $\sim 40\%$ is between the LAE LF realizations of $\alpha = -2.1$ and -2.2 . The likelihood falls for greater slopes: for the realization $\alpha = -2.5$ the LAE fraction is 0.477 (~ 19 LAEs) and the probability of finding *as few* as 13 LAEs for a 40 object sample has decreased to (100-98) = 2%. In comparison with MNS2, the flat and modest slopes of -1.0 and -1.5 for the LAE LF — although compatible with the brighter data of Shimasaku et al. — produce too few LAEs and are ruled out by our 13 LAE detections, as is the -2.5 slope, which produces too many.

The result is a probability distribution that is close to Gaussian, with the mean value of $\alpha = -2.15$ and a standard deviation of 0.20. The 2σ value is reached at -1.75 , as expected, but the 2σ on the steep side comes in at -2.50 rather than -2.55 . The shot noise associated with this relatively small sample suggests a systematic error of ~ 0.1 in the slope.

The LAE LF with a faint-end slope of $\alpha = -2.15$ passes two other tests that show how well it fits the data. The first considers how well the percentage of *each* foreground population in our new data compares to values derived in MNS2 for the COSMOS field (where there are data for the foregrounds, as described in MNS2), but applied to both of the 2008 search fields. (In this paper we used that 2008 model as a starting point to set the Φ^* of each foreground.) With our best-fitting realization of slope $\alpha = -2.15$, the relative foreground contributions over the $\log F = -16.8$ to -17.7 range are 57% for

[O II] compared to observed 63% (1σ bounds 42% - 70%), 34% [O III] compared to observed 30% (23%-45%), and 9% for H α compared to observed 7% (4% to 16%). This validates the foreground model used to derive slopes for the LAE LF of $\alpha \sim -2.0$ in MNS2, that is, the parameters for the Schechter functions describe the foregrounds well.

The second test concerns the LAE-to-foreground ratio as a function of decreasing flux. Although we have simply gathered together all the LAEs and foreground galaxies in the flux interval and focused on a single parameter — the LAE fraction, we can learn something from Figure 3 about the distribution — the increasing fraction of LAE/foreground with decreasing flux. Again, the best fit LAE LF derived with the new data is in agreement this observed trend: brighter than $\log F = -17.0$, foreground galaxies in the model outnumber LAEs by 9 to 1. At $\log F = -17.0$ this ratio has dropped to 4.4 to 1, and at $\log F = -17.6$ ergs s $^{-1}$ cm $^{-2}$ LAEs are almost one-to-one with the foreground. For all the uncertainty in the fluxes, this is what the data of Figure 3 show.

4.2. Comparison with the Keck-DEIMOS results

In MNS3 the results of Keck-Deimos observations in 2011 and 2012 were presented and analyzed, including the first recovery of faint LAEs in MNS, 6 LAEs with fluxes between $F = 5 - 10 \times 10^{-18}$ ergs s $^{-1}$ cm $^{-2}$. A maximum likelihood technique was used to find a LF faint-end slope of $\alpha \sim -1.7$, shallower than found here, but the $\alpha \sim -2.0$ slope found in MNS2 using a statistical correction of the foreground contamination is within the 1σ uncertainty of the both MNS3 and the present result. The methodology used here to measure the faint-end slope is not easily applied to the MNS3 data, since there was a prioritization of DEIMOS targets — based on previous low-resolution IMACS spectroscopy — that favored objects that were narrowed-down to be either LAE or [O II] foreground over those without additional information following the original detection in the 2008 search data (see MNS3). Also, the LAEs found in MNS3 cover only the brighter part of this paper’s sample (see Figure 3), which means that the LAE fraction is expected to be smaller, 26% instead of 33% — according to the best-fit model we find here. Still, it appears that the result of MNS3 points to a flatter slope. We stress, however, that the derivation of a probable $\alpha = -2.15$ slope is completely compatible with the data and analysis of MNS3.

A strength of the present work is that the LAE and foreground spectra represent a nearly complete ($\sim 85\%$ of targeted objects) sample, randomly selected by the spatial constraints of the multislit mask technique, that should be unbiased. This simplifies the analysis here. The unbiased selection of targets, and the much larger sample of confirmed LAEs, makes the present work the best assessment of the faint LAE population to-date, providing the strongest constraint on the faint-end slope α of the LAE LF.

5. THE LAE POPULATION COULD BE THE DOMINANT SOURCE OF REIONIZING PHOTONS

At $z = 5.7$, our sample lies past the redshift of full reionization at $z = 6.0$ — our LAEs contribute to *maintaining* ionization by balancing recombination. However, because $z = 5.7$ and $z = 6.0$ are separated by only by 64 million years, and by an additional 200 Myr to $z = 7$, it is reasonable to believe that our sample is representative of the similar emission-line galaxies *within* the reionization epoch. Furthermore, since HI absorption seems to substantially attenuate the Ly α signal at

$z \gtrsim 7$ (see §1), observing LAEs at $z = 5.7$ may turn out to be the best epoch to study the properties of LAEs at earlier times.

In MNS2 we reviewed a number of issues that were related to the possibility that the faint-end slope of the LAE LF is steep, $\alpha \sim -2.0$, something that the present study confirms. In that discussion, the identification of these faint LAEs as systems of halo mass $10^{10} - 10^{11}$ M $_{\odot}$, at a space density equivalent to several objects per today’s L* galaxy, motivated our contention that these are the likely progenitor components of L* galaxies, and that these lower mass systems are the probable source of the metal enrichment of the IGM at this early epoch. In this connection, the resolved profiles of most of the Ly α sources we have presented in this paper are consistent with large outflow velocities of hundreds of kilometers per second, but a reliable measurement of outflow velocity requires an as-yet-unmeasured local-standard-of-rest.

Here we consider only the ramifications of this now well-measured faint-end slope of the LAE LF at $z = 5.7$ for the question of the sources of reionization of the IGM. In MNS1 and MNS2 we derived the star formation-rate-density required to maintain ionization at $z \sim 5.7$ from the LAE LF flux. The uncertain parameters for calculating this quantity are the production rate and escape fraction of Ly α and Lyman-continuum photons and the clumping factor of the IGM. MNS1 derived the equation for the critical luminosity density \mathcal{L} in Ly α required to maintain ionization at $z = 5.7$,

$$(1) \mathcal{L} = 3.0 \times 10^{40} \text{ ergs}^{-1} \text{ s}^{-1} \text{ Mpc}^{-3} \times \zeta \times \left(\frac{1+z}{6.7} \right)^3 \left(\frac{\Omega_b h_{70}^2}{0.047} \right)^2$$

where

$$(2) \zeta = C_6 (1 - 0.1 f_{Ly\alpha,0.1}) \left(\frac{f_{Ly\alpha,0.5}}{f_{Ly\alpha,0.1}} \right)$$

combines the clumping factor, the Ly α escape fraction, and the Lyman-continuum escape fraction, normalized to values of 6, 0.5, and 0.1, respectively. A value of $\zeta \approx 1$ represents current estimates of these values.

The rising LF for faint LAEs we have confirmed here is an important step towards showing that galaxies at $z = 5.7$ are capable of maintaining ionization and, by implication, that a similar population of low-mass, low dust galaxies made a substantial contribution to reionization at $z \gtrsim 7$, only ~ 300 Myr earlier. In Figure 4 we reframe Figure 12 of MNS2 with the new limits on the faint-end slope, confirming that such systems have played a substantial, perhaps dominant role in the ionization of the IGM. Figure 4 shows the luminosity-density in Ly α as a function of the limiting luminosity of the LAE LF that has been measured. The critical flux density, \mathcal{L} , from Eqn. (1), is shown for 10%, 50%, and 100% of the flux required for full ionization. The blue shaded region shows how 1σ limits on the faint-end slope map onto the reionization flux. Assuming a modest factor-of-three extrapolation in limiting luminosity of our faint-end slope, our observations already reach a level of $\sim 35\%$ of the critical density, and a factor of three further extrapolation brings us to the $\sim 55\%$ level.

A faint end slope $\alpha > -2.0$ is unphysical, of course, in the sense that extrapolation of this LF indefinitely is unbounded. However, there is no reason to suspect that the physics responsible for the steep interval found here — significantly steeper than for any lower-redshift sample of galaxies, continues to apply. A shallowing of the slope α or even a cutoff for much fainter LAEs would not be unexpected. Further-

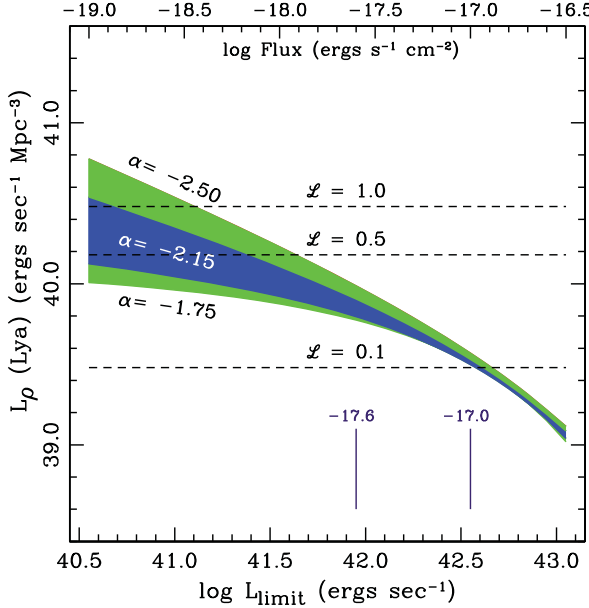


FIG. 4.— Level of luminosity density required for maintaining reionization at $z \approx 5.7$ with a population of faint LAEs. The blue and green shadings show the $\pm 1\sigma$ and $\pm 2\sigma$ bounds of a best-fit slope is $\alpha = -2.15$ and $\sigma = 0.20$. Within these limits, there is substantial progress toward reaching critical flux density, $\zeta = 1$: 22% is reached at the flux limit of our observations, 35% if the LF continues to a factor-of-three-fainter flux limit, and $\sim 56\%$ if it continues a full factor-of-ten. If the Lyman-continuum escape fraction reaches as high as 20%, the full reionizing budget could be reached at that point. Such a higher escape fraction is consistent with trends of increasing redshift and decreasing luminosity found in lower-redshift samples, increasing the likelihood that LAEs alone can provide the critical flux density to complete reionization at $z \sim 6$.

more, the steep slope we find for the LAE LF may not be entirely due to a steep increase in the actual number of objects, since an increasing Ly α escape-fraction, also not unexpected in lower-luminosity (lower-mass) systems (Schaerer

et al. 2011), could be partly responsible. Finally, we note that Figure 4 uses an escape fraction of Lyman-continuum photons of only 10%, a conservative value that may also be increasing with higher redshift and lower-mass systems (Hayes et al. 2011; Blanc et al. 2011; Nestor et al. 2011, 2013; Dijkstra & Jeeson-Daniel 2013; Jones et al. 2012; Jones et al. 2013; Cassata et al. 2014). If so, reaching the full flux needed to maintain or drive reionization may be achieved with a continuation of the steep LF for only a factor-of-ten beyond the luminosity range covered in this study. This contrasts with the situation described in Robertson and Ellis (2012) and Robertson et al. (2013) where an extrapolation of a factor of 100 to $M_{UV} = -13$ or fainter was required for Lyman-break galaxies.

6. CONCLUSION

We have confirmed a steep slope of Lyman- α emitters at $z = 5.7$ by finding a $\sim 32\%$ fraction of LAEs in a sample of 40 extremely faint emission-line galaxies. A robust test shows that this fraction of LAEs is inconsistent with faint-end slopes much flatter than $\alpha = -1.90$, and that a slope of $\alpha = -2.0$ or greater has a high probability. A slope this steep suggests a substantial, perhaps dominant contribution by LAEs to maintaining reionization at this epoch, with a moderate extension of the $\alpha \approx -2.0$ slope by a factor of ~ 10 or to fainter systems needed account for much or even all the required flux. Considering the proximity in time of these LAEs to objects within the reionization epoch, it is reasonable to imagine that similar emission-line galaxies at $z > 7$ make a substantial contribution to reionization in the early universe.

7. ACKNOWLEDGMENTS

AH is supported by an appointment to the NASA Postdoctoral Program at the Goddard Space Flight Center, administered by Oak Ridge Associated Universities through a contract with NASA.

REFERENCES

Alavi, A., Siana, B., Richard, J., et al. 2014, ApJ, 780, 143
 Blanc, G. A., Adams, J. J., Gebhardt, K., et al. 2011, ApJ, 736, 31
 Bouwens, R. J., Illingworth, G. D., Oesch, P. A., et al. 2014, arXiv:1403.4295
 Bradley, L. D., Trenti, M., Oesch, P. A., et al. 2012, ApJ, 760, 108
 Bunker, A. J., Wilkins, S., Ellis, R. S., et al. 2010, MNRAS, 409, 855
 Bunker, A. J., Caruana, J., Wilkins, S. M., et al. 2013, MNRAS, 430, 3314
 Caruana, J., Bunker, A. J., Wilkins, S. M., et al. 2012, MNRAS, 427, 3055
 Caruana, J., Bunker, A. J., Wilkins, S. M., et al. 2014, MNRAS, 443, 2831
 Cassata, P., Tasca, L. A. M., Le Fevre, O., et al. 2014, arXiv:1403.3693
 Curtis-Lake, E., McLure, R. J., Pearce, H. J., et al. 2012, MNRAS, 422, 1425
 Dijkstra, M., & Jeeson-Daniel, A. 2013, MNRAS, 435, 3333
 Dijkstra, M., Wyithe, S., Haiman, Z., Mesinger, A., & Pentericci, L. 2014, MNRAS, 440, 3309
 Dressler, A., Martin, C. L., Henry, A., Sawicki, M., & McCarthy, P. 2011a, ApJ, 740, 71, MNS2
 Dressler, A., et al. 2011b, PASP, 123, 288
 Dunlop, J. S., Rogers, A. B., McLure, R. J., et al. 2013, MNRAS, 432, 3520
 Ellis, R. S., McLure, R. J., Dunlop, J. S., et al. 2013, ApJ, 763, L7
 Fontana, A., Vanzella, E., Pentericci, L., et al. 2010, ApJ, 725, L205
 Hayes, M., Schaerer, D., Östlin, G., et al. 2011, ApJ, 730, 8
 Henry, A. L., Martin, C. L., Dressler, A., Sawicki, M., & McCarthy, P. 2012, ApJ, 744, 149
 Hu, E. M., Cowie, L. L., Barger, A. J., et al. 2010, ApJ, 725, 394
 Jones, T. A., Ellis, R. S., Schenker, M. A., & Stark, D. P. 2013, ApJ, 779, 52
 Jones, T., Stark, D. P., & Ellis, R. S. 2012, ApJ, 751, 51
 Kashikawa, N., et al. 2011, ApJ, 734, 119
 Kelson, D. D. 2003, PASP, 115, 688
 Kornei, K. A., Shapley, A. E., Erb, D. K., et al. 2010, ApJ, 711, 693
 Martin, C. L., Sawicki, M., Dressler, A., & McCarthy, P. 2008, ApJ, 679, 942, MNS1
 Marzke, R. O., Geller, M. J., Huchra, J. P., & Corwin, H. G., Jr. 1994, AJ, 108, 437
 McLure, R. J., Dunlop, J. S., Bowler, R. A. A., et al. 2013, MNRAS, 432, 2696
 Momose, R., Ouchi, M., Nakajima, K., et al. 2014, MNRAS, 442, 110
 Nestor, D. B., Shapley, A. E., Kornei, K. A., Steidel, C. C., & Siana, B. 2013, ApJ, 765, 47
 Nestor, D. B., Shapley, A. E., Steidel, C. C., & Siana, B. 2011, ApJ, 736, 18
 Oesch, P. A., Bouwens, R. J., Illingworth, G. D., et al. 2014, ApJ, 786, 108
 Ono, Y., Ouchi, M., Mobasher, B., et al. 2012, ApJ, 744, 83
 Ouchi, M., et al. 2008, ApJS, 176, 301
 Pentericci, L., Fontana, A., Vanzella, E., et al. 2011, ApJ, 743, 132
 Robertson, B. E., & Ellis, R. S. 2012, ApJ, 744, 95
 Robertson, B. E., Furlanetto, S. R., Schneider, E., et al. 2013, ApJ, 768, 71
 Schaerer, D. 2014, arXiv:1407.2796
 Schaerer, D., de Barros, S., & Stark, D. P. 2011, A&A, 536, A72
 Schenker, M. A., Stark, D. P., Ellis, R. S., et al. 2012, ApJ, 744, 179
 Schmidt, K. B., Treu, T., Trenti, M., et al. 2014, ApJ, 786, 57
 Shapley, A. E., Steidel, C. C., Pettini, M., & Adelberger, K. L. 2003, ApJ, 588, 65
 Shimasaku, K., et al. 2006, PASJ, 58, 313
 Stark, D. P., Ellis, R. S., Chiu, K., Ouchi, M., & Bunker, A. 2010, MNRAS, 408, 1628
 Stark, D. P., Schenker, M. A., Ellis, R., et al. 2013, ApJ, 763, 129
 Takahashi, M. I., et al. 2007, ApJS, 172, 456
 Taniguchi, Y., et al. 2007, ApJS, 172, 9
 Tilvi, V., Papovich, C., Finkelstein, S. L., et al. 2014, arXiv:1405.4869

TABLE 1
IDENTIFIED LAES AT $z = 5.7$

#	Identification	RA (2000.0)	DEC (2000.0)	$\lambda_{\text{Ly}\alpha}$ angstroms	Flux $\times 10^{18}$ ergs $\text{s}^{-1} \text{cm}^{-2}$
1	14.5+3-0.91	15:23:00.333	-00:13:28.18	8199	11.5
2	17.5-2-0.18	15:23:12.900	-00:15:33.56	8196	8.7
3	54.5+6-0.43	15:23:08.617	-00:01:24.37	8146	7.8
4	58.5+5-0.94	15:23:18.792	-00:02:31.55	8167	7.0
5	40.5-4-0.95	15:23:43.210	-00:15:01.20	8127	6.1
6	31.5+6-0.66	15:22:56.159	-00:06:23.60	8157	5.0
7	44.5+4-0.54	15:23:12.015	-00:05:46.11	8192	4.6
8	63.5+8-0.92	15:23:08.087	+00:01:53.87	8121	4.6
9	13.5+3-0.45	15:22:58.690	-00:13:24.69	8201	4.0
10	55.5-5-0.43	15:23:57.310	-00:13:16.30	8157	3.5
11	32.5-2-0.74	15:23:27.052	-00:13:47.32	8147	3.3
12	46.5-5-0.75	15:23:51.911	-00:15:05.34	8141	2.6
13	56.5-4-0.68	15:23:53.999	-00:12:04.48	8221	1.9

TABLE 2
SHIMASAKU ET AL. LAE LF MODELS AND MNS2 LAE LF REALIZATIONS

model LF _{LAE} α, L^*, Φ^*	R_{model} N(-17.6)/N(-17.3)	$R_{realization}$ N(-17.6)/N(-17.3)	[O II]	Foreground LF parameters		H α
				[O III]		
-1.0, 42.72, -2.92	1.621	1.628	[-1.44, 41.47, 0.768]	[-1.69, 41.42, -0.172]	[-1.69, 41.49, -1.392]	
-1.5, 42.90, -3.20	1.895	1.891	[-1.39, 41.52, 0.773]	[-1.68, 41.42, -0.080]	[-1.67, 41.49, -1.287]	
-2.0, 43.20, -3.80	2.284	2.286	[-1.30, 41.48, 0.836]	[-1.60, 41.42, -0.134]	[-1.60, 41.49, -1.303]	

NOTE. — (1) LF_{LAE} Schechter function parameters from Shimasaku et al. (2006); (2) ratio of integrated LAE counts, $N(\log F > -17.6 \text{ ergs s}^{-1} \text{cm}^{-2})/N(\log F > -17.3 \text{ ergs s}^{-1} \text{cm}^{-2})$, for Shimasaku et al. model, and (3) for MNS2 data realization; (4) Foreground LFs: Schechter parameters $[\alpha, \log L^*, \log \Phi^*]$

TABLE 3
LF FUNCTION FITS AND PROBABILITIES

model LF _{LAE} α, L^*, Φ^*	R_{model} N(-17.6)/N(-17.3)	$R_{realization}$ N(-17.6)/N(-17.3)	Foreground [O II] LF α, L^*, Φ^*	LAE fraction LAE/(LAE+fore)	LAEs expected	Monte Carlo n = 13	Probability %
-1.0, 42.72, -2.92	1.621	1.628	-1.44, 41.47, 0.768	0.099	4.0	1.0E-4	0.01%
-1.5, 42.90, -3.20	1.895	1.891	-1.45, 41.52, 0.790	0.142	5.7	1.9E-3	0.19%
-1.6, 42.95, -3.30	1.959	1.957	-1.39, 41.49, 0.796	0.151	6.0	3.2E-3	0.32%
-1.7, 43.01, -3.40	2.029	2.027	-1.39, 41.49, 0.804	0.177	7.1	0.015	1.5%
-1.8, 43.07, -3.52	2.105	2.107	-1.39, 41.49, 0.812	0.198	7.9	0.039	3.9%
-1.9, 43.13, -3.65	2.171	2.171	-1.39, 41.49, 0.822	0.218	8.7	0.076	7.6%
-2.0, 43.20, -3.80	2.284	2.286	-1.30, 41.48, 0.836	0.260	10.4	0.224	22%
-2.1, 43.28, -3.95	2.392	2.391	-1.21, 41.41, 0.754	0.285	11.4	0.345	35%
-2.2, 43.36, -4.12	2.506	2.508	-1.17, 41.41, 0.756	0.302	12.1	0.550	45%
-2.3, 43.45, -4.30	2.637	2.639	-1.16, 41.41, 0.712	0.363	14.5	0.741	26%
-2.4, 43.54, -4.50	2.783	2.781	-1.11, 41.41, 0.680	0.416	16.6	0.907	9.1%
-2.5, 43.63, -4.71	2.944	2.944	-1.05, 41.38, 0.593	0.477	19.1	0.981	2.0%

NOTE. — (1) LF_{LAE} Schechter function parameters based on Shimasaku et al. (2006); (2) ratio of integrated LAE counts, $N(\log F > -17.6 \text{ ergs s}^{-1} \text{cm}^{-2})/N(\log F > -17.3 \text{ ergs s}^{-1} \text{cm}^{-2})$ for Shimasaku et al. model, and (3) for MNS2 data realization; (4) LF_{OII} Schechter function parameters; (5) LAE fraction over flux interval $17.6 > \log F > -17.3$; (6) expected number of LAEs; (7) fraction of cases in Monte Carlo test with 13 LAEs and 27 foreground; (8) Probability of LF_{LAE} slope α .